CHEMISTRY OF MATERIALS

Article

pubs.acs.org/cm

First-Principles Studies on Cation Dopants and Electrolyte|Cathode Interphases for Lithium Garnets

Lincoln J. Miara,*[,†] William Davidson Richards,[‡] Yan E. Wang,[‡] and Gerbrand Ceder[‡]

[†]Samsung Advanced Institute of Technology—USA, 255 Main St., Suite 702, Cambridge, Massachusetts 02142, United States

[‡]Department of Materials Science and Engineering, Massachusetts Institute of Technology, 77 Massachusetts Ave., Cambridge, Massachusetts 02139, United States

Supporting Information

ABSTRACT: Lithium garnet with the formula $Li_7La_3Zr_2O_{12}$ (LLZO) has many properties of an ideal electrolyte in all-solid state lithium batteries. However, internal resistance in batteries utilizing these electrolytes remains high. For widespread adoption, the LLZO's internal resistance must be lowered by increasing its bulk conductivity, reducing grain boundary resistance, and/or pairing it with an appropriate cathode to minimize interfacial resistance. Cation doping has been shown to be crucial in LLZO to stabilize the higher conductivity cubic structure, yet there is still little understanding about which cations have high solubility in LLZO. In this work, we apply density functional theory (DFT) to calculate the defect energies and site preference of all possible dopants in these materials. Our findings suggest several novel dopants such as Zn^{2+} and Mg^{2+} predicted to be stable on the Li- and Zr-sites, respectively. To understand the source of interfacial resistance between the electrolyte and the cathode, we investigate the thermodynamic stability of the electrolyte|cathode interphase, calculating the reaction energy for LLMO (M = Zr, Ta) against $LiCoO_2$, $LiMnO_2$, and $LiFePO_4$ (LCO, LMO, and LFP, respectively) cathodes over the voltage range seen in lithium-ion battery operation. Our results suggest that, for LLZO, the LLZO|LCO is the most stable, showing only a low driving force for decomposition in the charged state into La_2O_3, $La_2Zr_2O_7$, and Li_2CoO_3, while the LLZO|LFP appears to be the most reactive, forming Li_3PO_4, $La_2Zr_2O_7$, $LaFeO_3$, and Fe_2O_3. These results provide a reference for use by researchers interested in bonding these electrolytes to cathodes.

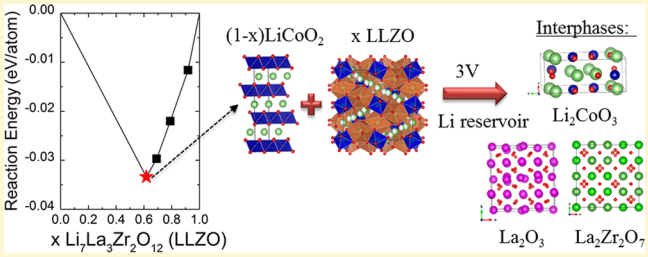

1. INTRODUCTION

The lithium-stuffed garnet with a nominal composition of $Li_7La_3Zr_2O_{12}$ (LLZO) has garnered significant attention in recent years, because of its stability toward lithium metal, wide electrochemical stability window, and modestly high ionic conductivity.[1−3] However, the internal resistance of the garnet electrolyte is still too high for use in a practical battery; depending on the material type and synthesis conditions, this resistance can be dominated by the bulk resistivity (due to bulk Li-ion mobility), grain-boundary resistance, or interfacial resistance between the electrodes and the electrolyte.[4−8]

The highest lithium-ion conductivity is found with the cubic phase (space group $Ia\bar{3}d$) of $Li_7La_3Zr_2O_{12}$ garnet.[9] However, at this concentration, a low-energy ordering of Li into the 8a (tetrahedral) and 16f, 32g (octahedral) sites of the tetragonal structure, can occur, reducing symmetry to $I4_1/acd$. The room-temperature ionic conductivity of the tetragonal structure is low, on the order of 10^{-6} S cm^{-1}, but the conductivity can be improved by over 2 orders of magnitude if the lithium ordering is broken and the cubic structure restored.[10] This is usually accomplished by creating Li vacancies through supervalent cation doping such as Al^{3+}, Ga^{3+}, on the Li-site or Ta^{5+}, Nb^{5+} on the Zr-site. Bernstein et al. showed that, beyond a critical vacancy concentration (x = 0.2 in $Li_{7-2x}A_xLa_3Zr_2O_{12}$, A = Al^{3+}, Ga^{3+}), the cubic structure is stabilized.[11] Recently, it was shown that Ta^{5+} ($x \geq 0.4$ in $Li_{7-x}La_3Zr_{2-x}Ta_xO_{12}$) doped onto the Zr-site is also efficient in stabilizing the cubic structure.[12] Achieving a sufficiently high vacancy concentration to disrupt the ordering significantly improves conductivity, regardless of the specific dopant or doping site used. Another method to increase conductivity and stabilize the cubic structure is to break the ordering by stuffing lithium into the garnet beyond 7 Li per formula unit (pfu).[13] Based on the available evidence, any dopant can lead to high conductivity if it has a high solubility within the host LLZO, and changes the lithium concentration away from 7 Li pfu. Many dopants have been tried by researchers (Ta^{5+}, Nb^{5+}, Al^{3+}, Ga^{3+}, In^{3+}, Sn^{4+}, Sb^{4+}, Y^{3+}, Ge^{4+}, Si^{4+}, Ca^{2+}, Sr^{2+}, Ba^{2+}, Hf^{4+}),[2,9,10,14−25] and for some of these, significant effort has gone into determining on which host site these dopants substitute.[26−30] For example, NMR studies and first-principles calculations have shown that Al^{3+} and Ga^{3+} reside on the Li-site.[14,29,31,32] However, for other dopants the most stable site in the LLZO structure has not been identified. In this work, we contribute to the body of

Received: March 18, 2015
Revised: April 30, 2015
Published: April 30, 2015

DOI: 10.1021/acs.chemmater.5b01023
Chem. Mater. 2015, 27, 4040−4047

Table 1. Elements and Oxidation States (Shown in Parentheses) of the Dopant Used in the Calculations[a] (128 total)

H(1)																He
Li(1)	Be(2)											B(3)	C(4)	N(3,5)	O	F	Ne
Na(1)	Mg(2)											Al(3)	Si(4)	P(3,5)	S(2,4)	Cl(1,3,5)	Ar
K(1)	Ca(2)	Sc(3)	Ti(4)	V(5)	Cr(3)	Mn(2,4)	Fe(2,3)	Co(2,3)	Ni(2)	Cu(2)	Zn(2)	Ga(3)	Ge(2,4)	As(3,5)	Se(2,4)	Br(1,3,5)	Kr
Rb(1)	Sr(2)	Y(3)	Zr(4)	Nb(5)	Mo(4)	Tc(4)	Ru(3,4)	Rh(3)	Pd(2,4)	Ag(1)	Cd(2)	In(3)	Sn(2,4)	Sb(3,5)	Te(2,4)	I(1,3,5)	Xe
Cs(1)	Ba(2)	Lu(3)	Hf(4)	Ta(5)	W(4)	Re(4)	Os(4)	Ir(3,4)	Pt(2,4)	Au(3)	Hg(1,2)	Tl(1,3)	Pb(2,4)	Bi(3)	Po(2,4)	At(1)	Rn
Fr(1)	Ra(2)	Lr(3)															
	La(3)	Ce(3,4)	Pr(3)	Nd(3)	Pm(3)	Sm(3)	Eu(2,3)	Gd(3)	Tb(3)	Dy(3)	Ho(3)	Er(3)	Tm(3)	Yb(3)			
	Ac(3)	Th(4)	Pa(5)	U	Np(5)	Pu(4)	Am(3)	Cm(3)	Bk(3)	Cf(3)	Es(3)	Fm(3)	Md(3)	No(3)			

[a]A total of 128 were used.

knowledge on doped garnets by calculating the defect energy and site preference of these and many other potential dopants from first-principles.

Despite high bulk conductivity, any electrolyte is impractical if a large interfacial resistance is present, arising from decomposition products formed between the cathode and the electrolyte at high sintering temperatures, or from electrochemical decomposition at the interface during cycling. In this context it is the formation of a resistive interphase layer at the interface that leads to the observed resistance. Therefore, a careful analysis of the phases present may provide insight into those interested in reducing the observed interfacial resistance. Phase-decomposition arises from the unequal chemical potentials between the different atomic species across the interface. Rapid decomposition is seen for the sulfide electrolyteloxide cathode combination, and thus a blocking layer is almost universally employed between the cathode and electrolyte.[33] The problem of interfacial resistance has also been documented for the LLZO system.[34] These researchers report poor performance in all-solid-state batteries with LLZO electrolyte and LCO cathodes caused by a co-diffusion of La, Zr, and Co, leading to increased interfacial resistance, although it is unclear if this is from sintering or decomposition during charging.

In this work, we use first-principles calculations to identify the thermodynamic driving forces for decomposition reactions between the electrolyte and electrode over the voltage range experienced during operation. We examine LLZO and the similar material, $Li_5La_3Ta_2O_{12}$ (LLTO),[21,35] against three common cathodes: LCO, LMO, and LFP. We perform a careful thermodynamic assessment of the interphase equilibrium using a Grand Canonical ensemble open to lithium. As the lithium chemical potential is changed (i.e., simulating charge/discharge), the reaction energy for the formation of the lowest energy equilibrium of interphases from mixing of the cathode and electrolyte composition is determined. Together with the dopant stability analysis, we provide valuable information when choosing a system for all-solid-state battery construction using LLZO or LLTO as an electrolyte.

2. DOPANT STABILITY

2.1. Stability Calculation Methodology. In our dopant study, we consider 128 possible dopant species (Table 1), each of which can be placed at three cation sites (Li, La, Zr). In addition, there are 3 lithium sites (24d, 96h, 48g) which must also be tested when a dopant is placed on the Li-site, leading to a total of 1152 structures to be calculated. Some cations are clearly less probable than others, such as placing 6+ cations on the La-site or 1+ substitution on the Zr-site. Many can be ruled out simply in terms of ionic radii or coordination number; however, they are included in this work for completeness. For compounds in which the doping would lead to unbalanced charge, the Li concentration is adjusted to maintain charge neutrality. For example, when Al^{3+} is placed on a Li site, three Li^+ ions are removed. Li atoms are removed (as vacancies) from the highest energy sites or added (as interstitials) to the lowest energy sites, according to an electrostatic energy criterion.[36]

The oxidation states of the dopants range from 1+ to 6+ and are placed on the Li^+, La^{3+}, and Zr^{4+} sites in LLZO, creating structures with a range of Li concentration from $Li_{6.25}A_{0.125}La_3Zr_2O_{12}$ to $Li_{7.375}La_3Zr_{1.875}M_{0.125}O_{12}$ (A = 6+ dopant on Li site, M = 1+ dopant on Zr-site, respectively). The defect formation energy is calculated as

$$E_{\text{defect}} = E_{\text{pure}} - E_{\text{doped}} + \sum_{N}^{i} \Delta n_i \mu_i \quad ([1])$$

where E_{doped} and E_{pure} are the total energy of the supercell with and without the dopants, respectively; Δn_i is the number of atoms of element i added to (or removed from) the supercell to create and charge balance the supercell; and μ_i is the chemical potential of element i. This is summed for all elements N, which are added or removed during the doping reaction. The chemical potentials for each element i are determined from the multiphase equilibrium that contains the composition of the doped structure. This is calculated as the slope in the direction of element i in the phase diagram. The software suite pymatgen is used to generate the phase diagram and calculate the chemical potentials of the elements added or removed during the reaction.[37]

To compute the relevant phase diagrams that are needed to obtain the chemical potentials of defect species in the defect energy computations and the reaction products in the interfacial stability calculations, we obtained relevant structures from the International Crystal Structure Database (ICSD),[38] and from our internal database of structures generated with data-mined substitution rules.[39] All compounds in a given quintenary system Li−La−Zr−O−M (where M = dopant) were calculated.

We calculated the ground state of the garnet structure, starting with the disordered structure from the ICSD (CC:

DOI: 10.1021/acs.chemmater.5b01023
Chem. Mater. 2015, 27, 4040−4047

422259) but adopted site occupancy factors (SOFs) of 0.417 for Li(1) and 0.479 for Li(2), for the 8-formula-unit conventional supercell, which are more consistent with recent experimental and computational works.[3,40] This structure with space group $Ia\bar{3}d$ (No. 230) is disordered on both the 24d Li(1) tetrahedral site and the 96h Li(2) octahedral sites. As the structure has partial occupancies for Li^+, we screened the possible arrangements of Li atoms by first applying an electrostatic energy criterion.[36] Based on this criterion, there were no occupied nearest-neighbor 24d and 96h sites. We calculated the energies of the 100 orderings with the lowest electrostatic energy using DFT, taking the structure with the lowest DFT energy as the ground-state structure.

All density functional theory (DFT) calculations were performed in the Perdew–Burke–Ernzerhof (PBE) generalized-gradient approximation (GGA),[41] implemented in the Vienna Ab initio Simulation Package (VASP).[42] The projector augmented-wave (PAW)[43] method is used for representation of core states. An energy cutoff of 500 eV and a *k*-point density of at least 1000/(number of atoms in the unit cell) was used for all computations.

2.2. Stability Analysis Results. The most common dopant for LLZO is Al^{3+}, either intentionally or from the crucible during calcination,[32] so we use Al^{3+} to illustrate our methods. The first step is to determine which cation site is most favorable for Al^{3+} doping. To do this, we placed the Al^{3+} ion into each of the cation sites and performed a charge balance according to the following:

Al^{3+}(Li):

$$Li_{56}La_{24}Zr_{16}O_{96} + Al^{3+}(Li) - 3Li \rightarrow Li_{53}AlLa_{24}Zr_{16}O_{96}$$

Al^{3+}(La):

$$Li_{56}La_{24}Zr_{16}O_{96} + Al^{3+}(La) - La \rightarrow Li_{56}La_{23}AlZr_{16}O_{96}$$

Al^{3+}(Zr):

$$Li_{56}La_{24}Zr_{16}O_{96} + Al^{3+}(Zr) + Li - Zr \rightarrow Li_{57}La_{24}Zr_{15}AlO_{96}$$

For convenience, the notation adopted here is Al^{3+}(Li), indicating Al^{3+} doped on the Li-site; accordingly, the other sites are denoted as Al^{3+}(La) and Al^{3+}(Zr). In the case of Al^{3+}(Li) substitution, the calculated quintenary phase diagram predicts the doped garnet to decompose into La_2O_3, Li_5AlO_4, and $La_6Zr_2O_7$, as shown in Figure 1. The defect energies and decomposition products for all sites are

Al^{3+}(Li):

$$Li_{53}AlLa_{24}Zr_{16}O_{96} \rightarrow Li_5AlO_4 + 8Li_6Zr_2O_7 + 12La_2O_3$$

$$E_{defect} = 1.36\ eV$$

Al^{3+}(La):

$$Li_{56}La_{23}AlZr_{16}O_{96} \rightarrow 0.6Li_8ZrO_6 + Li_5AlO_4 + 7.7Li_6Zr_2O_7 + 11.5La_2O_3 \qquad E_{defect} = 3.16\ eV$$

Al^{3+}(Zr):

$$Li_{57}La_{24}Zr_{15}AlO_{96} \rightarrow 1.4Li_8ZrO_6 + Li_5AlO_4 + 6.8Li_6Zr_2O_7 + 12La_2O_3 \qquad E_{defect} = 1.87\ eV$$

The lowest defect energy for Al^{3+} incorporation is found for Al^{3+}(Li), which is in good agreement with magic angle spinning (MAS) nuclear magnetic resonance (NMR) spectroscopy, which locates the Al^{3+} on the Li-sites.[29,32,44] Furthermore, our work is in perfect agreement with a recent in-depth computational analysis, regarding the location of the Al^{3+} in the cubic structure, which showed the order of site preference was Li (24d tetrahedral site) > Li (96h octahedral site) > Zr (16a) ≫ La (24c).[45] The complete set of results for all dopants is provided in the Supporting Information (Table S3) and is summarized in Figure 2. It is interesting to note that we predict that, of the 3d transition metals, only Fe^{3+}(Li) has a lowest energy site on Li; the others all favor the Zr-site, in excellent agreement with recent findings.[46]

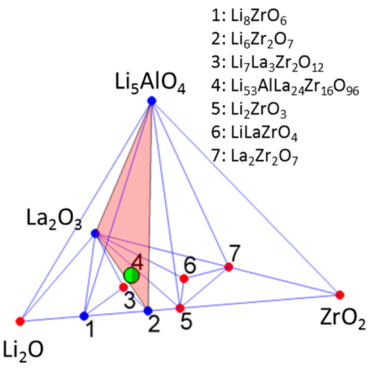

Figure 1. A quaternary section of the quintenary phase diagram for Li–La–Al–Zr–O. The position of the new compound, $Li_{53}AlLa_{24}Zr_{16}O_{96}$, is highlighted in green in the decomposition triangle. This particular substitution has a defect energy of 1.36 eV.

The solubility of a dopant is primarily a function of its defect energy, with that defect energy compensated by the increased entropy due to Li disorder. Determination of the exact entropic contribution for each dopant is beyond the scope of this research; therefore, as an approximation of what may be synthesized, we determine the dopant that has been successfully synthesized with the highest calculated defect energy. According to our results and past literature of which we are aware, Ce^{4+}(La) with E_{defect} = 1.60 eV is the highest[18] among the synthesized compounds; however, to broaden our search, we use Te^{6+}(Zr) with E_{defect} = 2 eV as a reasonable defect energy cutoff. Although, to the authors' knowledge, doping LLZO with Te has not been attempted in the past, solid solutions of Te compounds were successfully synthesized in the related $Li_{3+x}Nb_3Te_{2-x}Sb_xO_{12}$ ($0.05 \le x \le 1.5$) series.[47]

The number of possible defects on each site, after filtering with a defect energy cutoff of 2 eV, is summarized in Table 2, and the list of dopants can be found in the Supporting Information (Table S2). In applying this filter, dopants are allowed to be stable on multiple sites and in multiple oxidation states. From this analysis, there are 37 dopant(site) combinations that are isovalent with the doped site, and while they likely have high solubility, they will not modify the Li concentration and, therefore, are unlikely to stabilize the cubic structure (highlighted blue in Table S2 in the Supporting Information). Of the remaining combinations, 25 contain 3*d* transition metals. Recent experimental work has demonstrated that Fe^{3+} doping is effective at stabilizing the cubic structure,[31,46] but 3*d* transition metals are generally not suitable for electrolytes, since the 3*d* transition-metal cations can be reduced against the lithium anode. After removing V, Cr, Mn, Fe, Co, and Ni, highlighted in red in Table S2 in the Supporting Information, there remain 59 dopant(site) stable combinations

DOI: 10.1021/acs.chemmater.5b01023
Chem. Mater. 2015, 27, 4040–4047

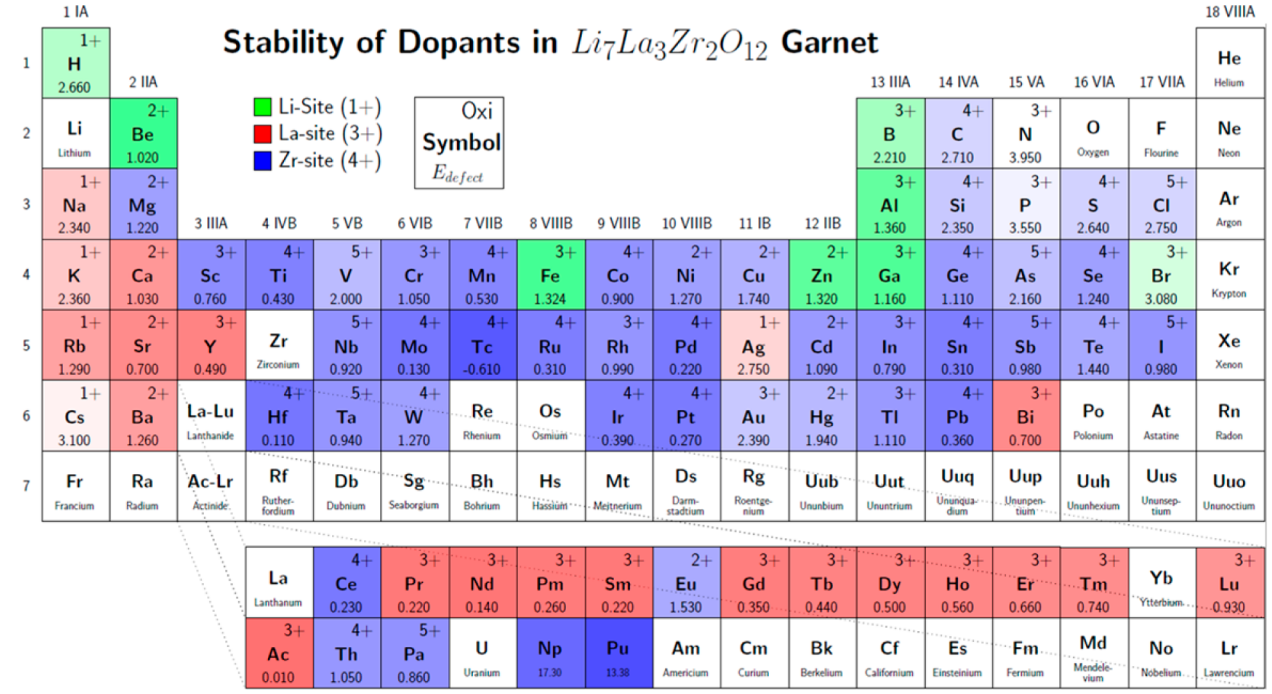

Figure 2. Site and oxidation state preference for the dopant elements studied. The color shows the most stable cation site (green for Li-site, red for La-site, and blue for Zr-site). The darker colors signify lower defect energy, such that Al^{3+}(Li) is darker than B^{3+}(Li). The box also shows the preferred oxidation state and the defect energy (in eV).

Table 2. Number of Dopant(Site) Combinations for LLZO with a Calculated Defect Energy of <2 eV[a]

site	total	subvalent	isovalent	supervalent
Li(1+)	15(10)	0	0	15(10)
La(3+)	27(25)	7(7)	18(18)	2(2)
Zr(4+)	66(57)	36(30)	19(17)	11(10)

[a]The results after excluding 3*d* transition-metal dopants are shown in parentheses.

that are not isovalent with the host site, marked as the numbers in parentheses in Table 2.

The highest conductivities are usually seen between 6−7 Li pfu.[25,48] Supervalent dopants are required to achieve these concentrations in LLZO, and, as was mentioned in the Introduction, the most common dopants are Al^{3+}(Li), Ga^{3+}(Li), Ta^{5+}(Zr), and Nb^{5+}(Zr). From our analysis, we identify several more low-energy dopants that are not 3*d* transition metals, and are relatively Earth-abundant. Perhaps the most interesting is Zn^{2+}(Li) with a defect energy of 1.32 eV, which is slightly lower than Al^{3+}(Li). Zn is further attractive, since it is a common component of solid electrolytes.[49−51] Other possibilities include Mg^{2+}(Li), Sb^{5+}(Zr), W^{6+}(Zr), and Mo^{6+}(Zr), which all have defect energies below the 2 eV cutoff.

Subvalent dopants leading to compositions with Li above 7 pfu have typically been avoided in the past. However, we have previously shown that Rb^{1+}(La), with calculated defect energy of 1.29 eV, stabilizes the cubic structure and has high conductivity.[3] From Table 2 it is seen that there are 30 subvalent non-3*d* transition-metal dopants on the Zr-site below the threshold. Many of these dopants are Earth-abundant and have defect energies similar to or lower than Al^{3+}(Li). Some interesting dopants that do not appear to have been tried before include Mg^{2+}(Zr) (which has a defect energy of 1.22 eV), Sc^{3+}(Zr), Ca^{2+}(Zr), and Ca^{2+}(La). Therefore, two strategies are to combine two dopants to achieve a concentration of ∼6.5 Li pfu, or a renewed push to examine garnets with a lithium content of >7 Li pfu may yield novel compounds.

3. INTERPHASE THERMODYNAMICS

3.1. Interphase Calculation Methodology. Reaction between the electrolyte and cathode is common and may create undesirable interphase products. The thermodynamic driving force for this reaction can come either from the reduction in interfacial energy, or from the thermodynamics of mixing the two compositions to create new phases with a lower bulk free energy. We find that, for many electrolyte|cathode interfaces, the phase equilibrium thermodynamics of the bulk materials dominate any energy changes that could be expected from changes in interface energies. Thus, studying the interphases formed at the interface is accomplished by analyzing the phase diagram consisting of all the elements in the combined electrolyte + electrode materials. Since it is not known *a priori* in which ratio the electrolyte and electrode react, all compositions on the tie line between their relative compositions must be evaluated. To determine the interphases in a Li-ion battery, this equilibrium is complicated by the fact that there are sources and sinks for lithium, and all thermodynamic potentials must be evaluated in open-system conditions for a specified Li chemical potential (μ_{Li}).[37,52] Hence, we search for the composition on the tie line between the electrode and electrolyte composition, which results in the largest driving force for reaction at a given μ_{Li}.

For each composition c in a phase diagram, the lowest energy $E_{hull}(c)$ is obtained by evaluating the convex energy hull corresponding to the phase diagram at that composition. The convex hull gives, at any composition c, the linear combination of phases that corresponds to the lowest energy. Equilibrating

DOI: 10.1021/acs.chemmater.5b01023
Chem. Mater. 2015, 27, 4040−4047

this composition with a lithium reservoir leads to a grand potential φ_{hull}:

$$\varphi_{hull}(c, \mu_{Li}) = \min_{n_{Li}}[E_{hull}(c + n_{Li}) + n_{Li}\mu_{Li}] \quad (2)$$

where n_{Li} is the number of atoms transferred to/from the lithium reservoir. Then, at a constant μ_{Li}, we search for decomposition products along the tie line between electrolyte|cathode compositions, according to

$$\Delta\varphi(\mu_{Li}) = \min_{x\in[0,1]}\begin{bmatrix}\varphi_{hull}(xc_{electrolyte} + (1-x)c_{cathode}, \mu_{Li}) \\ -x\varphi_{hull}(c_{electrolyte}, \mu_{Li}) - (1-x)\varphi_{hull} \\ (c_{cathode}, \mu_{Li})\end{bmatrix} \quad (3)$$

where the reaction energy, $\Delta\varphi(\mu_{Li})$, is the driving force for reaction between the electrolyte and the cathode, and x is a mixing parameter corresponding to a point on the tie line between the electrolyte and electrode compositions. For each lithium chemical potential, the value of x is varied to find the reaction with the largest reaction energy. This calculation is performed over the voltage range of 0 to 5.0 V vs lithium metal (corresponding to -5 eV $< \mu_{Li} < 0$ eV vs lithium metal). We repeat this procedure for LLZO and LLTO electrolytes against three common cathode materials: LCO, LMO, and LFP.

To better understand the decomposition reactions, we also calculate the intrinsic stability windows of LLZO and LLTO garnets and cathodes. The intrinsic window is defined as the lithium chemical potential range over which the garnet phases are stable. One may think of this as the stability against an ideal electrode material that would not decompose but only release or absorb Li. This is important since, after electrolyte decomposition, the interface reactions occur between decomposed electrolyte and cathode. The process is similar to calculations made for $Li_{10}GeP_2S_{12}$ found elsewhere.[53] The procedure is to generate the lithium grand potential phase diagrams of Li−La−Zr−O and Li−La−Ta−O (and corresponding diagrams for the cathodes) from $\mu_{Li} = 0$ to -5 eV vs lithium metal (see Ong et al.[52] for more details).

3.2. Interphase Calculation Results. To demonstrate these methods, we use the example of LLZO|LCO. The complete quintenary (Li−La−Zr−Co-O) Grand Canonical phase diagram at 3 V is shown in Figure S1 in the Supporting Information, and the tie line between the two compounds is highlighted. It bears repeating that the stable phases will change with the voltage.[52] The largest reaction energy, according to eq 3, along this tie line represents the most likely decomposition phases. A pseudo-binary phase diagram for this interface at 3 V is shown in Figure 3, and the decomposition phase equilibria are labeled on the figure. It is seen that the reaction at $x = 0.618$ has the largest driving force, and the predicted decomposition products are La_2O_3, $La_2Zr_2O_7$, and Li_2CoO_3. In our analysis Li_2CoO_3 is a predicted material that has a similar structure to the well-known Li-excess material Li_2MnO_3, and is stable according to DFT calculations. The maximum reaction energy phases at 3 V for all cathodes and electrolytes studied are presented in Table 3, and the results at other voltages are presented in Table S1 in the Supporting Information.

From Table 3, it is observed that, at 3 V, the reactivity of LLZO/LLTO with the cathodes is $\Delta\varphi_{LFP} > \Delta\varphi_{LMO} > \Delta\varphi_{LCO}$, and, for all cathodes, LLZO is more reactive than LLTO. The main reaction involves lithium and oxygen loss from the electrolytes. For the reactions of LLZO/LLTO with LCO and LMO, the cathode gains lithium and is oxidized, forming Li_2MO_3 (M = Mn, Co). In LFP, the phosphorus has a strong tendency to gain lithium and form Li_3PO_4.

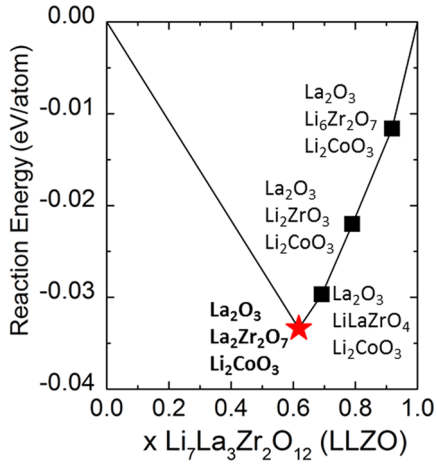

Figure 3. LLZO|LCO pseudo-binary phase diagram when Li is available at 3 V vs lithium metal. The decomposition products along the tie line are marked, and the maximum driving force reaction is marked with a red star.

The above routine (generate a tie line on the Grand Canonical phase diagram and find the largest reaction energy) is repeated for voltages from 0 to 5.0 V vs lithium metal and the results are plotted in Figure 4. The calculated intrinsic stability windows of the electrolytes and cathodes are marked at the bottom of Figure 4. It is seen that the LLZO is more stable at low voltages, but both garnets are decomposed by 3.8 V. Within the electrolyte stability window, the trends seen at 3 V largely hold. The biggest driving force for decomposition occurs at the edges of the intrinsic stability windows. LLTO is less reactive than the LLZO above 2 V against all cathodes. Above 3.8 V, the electrolyte decomposition products remain constant and so the lines are horizontal in Figure 4. Similarly at low voltages, in the cathode decomposition regime, the cathode decomposition products (i.e., metal and Li_2O) are stable against the electrolytes. The reaction energy is zero against LLZO. At voltages of <2 V, the LLTO begins to decompose to form Li_2O and metal alloys with the decomposing cathodes: $TaCo_3$, $TaMn_2$, (see Table S1 in the Supporting Information for complete decomposition products). However, these low voltages are not normally accessed at the electrolyte|cathode interface during battery operation, especially since they are outside of the cathode stability range.

4. DISCUSSION

Lithium-stuffed garnets can accommodate a wide array of dopant elements on all three cation sites. Doping is a successful strategy for improving conductivity by stabilizing the cubic structure. Most experimental evidence suggests that a lithium concentration of ~6.5 Li pfu shows the highest conductivity.[12] Thus, supervalent cations are typically used as dopants. The most commonly used dopant is Al^{3+}(Li); however, we find that (i) the defect energy of Al^{3+}(Li) is higher than several others and (ii) after a certain solubility limit, the formation of Li_5AlO_4, $Li_6Zr_2O_7$, and La_2O_3 is predicted. In contrast, Sn^{4+}(Zr) has a defect energy of 0.31 eV and is known to form the stable garnet compound $Li_7La_3Sn_2O_{12}$,[15] and a complete solid solution is expected. In this work, we find several promising subvalent

DOI: 10.1021/acs.chemmater.5b01023
Chem. Mater. 2015, 27, 4040−4047

Table 3. Maximum Reaction Energies and Decomposition Products Are Shown for the Electrolyte|Cathode Combinations Studied, with Li Available at 3 V

(x) electrolyte	$(1-x)$ cathode	$\Delta\varphi$ (meV/atom)	decomposition products
2.00 LLZO	7.02 LCO	−33.37	La_2O_3 + 2.000 $La_2Zr_2O_7$ + 7.000 Li_2CoO_3
2.01 LLZO	7.05 LMO	−108.9	La_2O_3 + 2.008 $La_2Zr_2O_7$ + 7.033 Li_2MnO_3
1.48 LLZO	3.47 LFP	−181.17	3.457 Li_3PO_4 + Fe_2O_3 + 1.481 $La_2Zr_2O_7$ + 1.469 $LaFeO_3$
1.00 LLTO	1.0 LCO	−10.54	Li_3TaO_4 + Li_2CoO_3+ La_3TaO_7
2.01 LLTO	5.07 LMO	−56.45	La_3TaO_7 + 5.039 Li_2MnO_3 + 3.026 $LaTaO_4$
1.00 LLTO	2.67 LFP	−124.41	$LaPO_4$ + 1.666 Li_3PO_4 + 1.334 Fe_2O_3 + 1.998

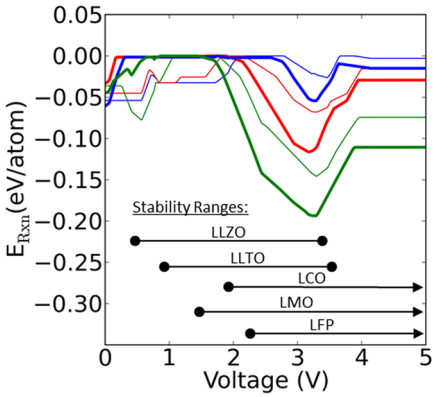

Figure 4. Driving force for interphase formation between electrolyte, and cathode, with varying voltage from 0 to 5 V vs lithium metal. [Legend: blue, LCO; red, LMO; green, LFP; thick line, LLZP; thin line, LLTO.] The calculated intrinsic stability windows are marked along the bottom for reference.

dopants with similar or lower defect energies, compared to Al^{3+}(Li), such as Zn^{2+}(Li), and Mg^{2+}(Li). Moreover, recent molecular dynamics simulations and experimental work suggests that LLZO compounds with Li concentrations above 7 pfu can also exhibit high conductivities.[13,54−56] This suggests a new path for stabilizing the cubic structure, since many of the low-defect-energy dopants from our calculations are subvalent dopants that increase the lithium concentration. In this group, the dopant(site) combinations with relatively low defect energies are Sc^{3+}(Zr), Ca^{2+}(Zr), Bi^{3+}(Zr), Mg^{2+}(Zr), Ca^{2+}(La), Sr^{2+}(La), and Ba^{2+}(La), many of which have been used with LLTO, but not LLZO. The others are listed in Table S2 in the Supporting Information.

In many cases, interfacial resistance between the cathode and electrolyte dominates the battery cell resistance and greatly reduces the cell power; however, finding a compatible interface is a difficult and time-consuming experimental process. Electrolyte|cathode interfacial resistance arises by chemical and electrochemical means. In this work, we propose a novel approach to study the electrochemical driving force for decomposition. By varying the voltage, the interphase formation between electrolyte|cathode are identified with the largest reaction energy (according to eq 3). Our results indicate LCO is a good choice, since it shows little reactivity toward the garnet electrolytes. On the other hand, the LFP cathode is more reactive with the garnet electrolytes; the Fe is oxidized forming the higher oxidation state phases, such as Fe_2O_3 and Li_3PO_4. In fact, we have checked several other $LiMPO_4$ (M=Ni, Cr, V) phases and this pattern holds. It is possible that, in reality, the Li_3PO_4 could form at the cathode|electrolyte interphase as a protective barrier layer and prevent further decomposition reactions, although this would require that the balance of the reaction products containing iron oxides does not create percolating electronic pathways.

Experimentally, there have been conflicting reports about the stability of the LLZO|LCO interface. Some reports show a large interfacial resistance with a heterogeneous layer at the interface containing Co, La, and Zr.[34,57] However, other reports show no evidence of interfacial resistance, even upon cycling.[58,59] From the information contained within Figures 2 and 4, it is possible to resolve this conflict. Co, La, and Zr ions are relatively large, and highly charged ions that are unlikely to diffuse at room temperature. However, when co-sintered at elevated temperatures, the thermodynamic driving forces lead to interdiffusion and decomposition. From the stability analysis (section 2.2), we predict decomposition of Co^{3+}(Zr) LLZO into La_2O_3, $Li_6Zr_2O_7$, and Li_8CoO_6 (Table S3 in the Supporting Information), in good agreement with Kim et al.,[57] who found evidence of decomposition at the LLZO|LCO interface.[60] On the other hand, low-temperature PLD deposition of LCO on LLZO showed stable cycling.[59] From Figure 4, this suggests a metastable interphase is formed. The stable cycling can be taken into consideration by the relatively low driving force for decomposition interphases between LLZO|LCO seen across the range of lithium chemical potentials studied in Figure 4, or the decomposed products act as a barrier layer, preventing further decomposition, as seen at high voltages. The effects on stability due to oxygen or lithium loss from the garnet during high-temperature sintering is beyond the scope of the current study, but they will be considered in future work.

Generally, our results support experimental findings[57,59] that the electrolyte|cathode interphase is more sensitive to chemical decomposition at high sintering temperatures than it is to electrochemical decomposition during cycling. This shows the importance and difficulty of careful synthesis, but also the promise of lithium garnets for use in all solid-state batteries.

5. CONCLUSIONS

In summary, we investigate the potential for finding stable cation dopants and mitigating internal resistance of $Li_7La_3Zr_2O_{12}$ (LLZO) garnet through first-principles calculations. We examine all possible cation dopant elements for LLZO and their site preference (Li, La, or Zr) by comparing the calculated defect energies. Several novel dopants emerge such as subvalent Sc^{3+} and Mg^{2+} on the Zr-site. The interphase resistance is studied by examining LLZO and $Li_5La_3Ta_2O_{12}$ (LLTO) electrolyte reactions with $LiCoO_2$ (LCO), $LiMnO_2$ (LMO), and $LiFePO_4$ (LFP) cathodes. We find that at high voltages the LMO and LFP react rather strongly with the garnet electrolytes, while the LCO is relatively stable. These results are a valuable resource for researchers looking to find stable cation dopants and cathodes to improve all solid-state battery performance with LLZO electrolytes bonded to cathodes.

DOI: 10.1021/acs.chemmater.5b01023
Chem. Mater. 2015, 27, 4040−4047

■ ASSOCIATED CONTENT

Supporting Information

The Supporting Information is available free of charge on the ACS Publications website at DOI: 10.1021/acs.chemmater.5b01023.

■ AUTHOR INFORMATION

Corresponding Author

*E-mail: Lincoln.m@samsung.com.

Notes

The authors declare no competing financial interest.

■ ACKNOWLEDGMENTS

The authors would like to thank Samsung Advanced Institute of Technology for funding support on this research. This work used computational resources provided by the Extreme Science and Engineering Discovery Environment (XSEDE), supported by the National Science Foundation (Grant No. ACI-1053575), and the National Energy Research Scientific Computing Center (NERSC), a DOE Office of Science User Facility supported by the Office of Science of the U.S. Department of Energy (under Contract No. DE-AC02-05CH11231).

■ REFERENCES

(1) Murugan, R.; Weppner, W.; Schmid-Beurmann, P.; Thangadurai, V. Structure and Lithium Ion Conductivity of Bismuth Containing Lithium Garnets $Li_5La_3Bi_2O_{12}$ and $Li_6SrLa_2Bi_2O_{12}$. *Mater. Sci. Eng., B* **2007**, *143* (1−3), 14−20.

(2) Murugan, R.; Ramakumar, S.; Janani, N. High Conductive Yttrium Doped $Li_7La_3Zr_2O_{12}$ Cubic Lithium Garnet. *Electrochem. Commun.* **2011**, 12−14.

(3) Xu, M.; Park, M. S.; Lee, J. M.; Kim, T. Y.; Park, Y. S.; Ma, E. Mechanisms of Li^+ Transport in Garnet-Type Cubic $Li_{3+x}La_3M_2O_{12}$ (M = Te, Nb, Zr). *Phys. Rev. B* **2012**, *85* (5), 1−5.

(4) Santhanagopalan, D.; Qian, D.; McGilvray, T.; Wang, Z.; Wang, F.; Camino, F.; Graetz, J.; Dudney, N.; Meng, Y. S. Interface Limited Lithium Transport in Solid-State Batteries. *J. Phys. Chem. Lett.* **2014**, *5* (2), 298−303.

(5) Dudney, N. J.; Neudecker, B. J. Solid State Thin-Film Lithium Battery Systems. *Curr. Opin. Solid State Mater. Sci.* **1999**, *4* (5), 479−482.

(6) Fergus, J. W. Ceramic and Polymeric Solid Electrolytes for Lithium-Ion Batteries. *J. Power Sources* **2010**, *195* (15), 4554−4569.

(7) Knauth, P. Inorganic Solid Li Ion Conductors: An Overview. *Solid State Ionics* **2009**, *180* (14−16), 911−916.

(8) Yashima, M.; Itoh, M.; Inaguma, Y.; Morii, Y. Crystal Structure and Diffusion Path in the Fast Lithium-Ion Conductor $La_{(0.62)}Li_{(0.16)}TiO_3$. *J. Am. Chem. Soc.* **2005**, *127* (10), 3491−3495.

(9) Murugan, R.; Thangadurai, V.; Weppner, W. Fast Lithium Ion Conduction in Garnet-Type $Li_7La_3Zr_2O_{12}$. *Angew. Chem., Int. Ed. Engl.* **2007**, *46* (41), 7778−7781.

(10) Shimonishi, Y.; Toda, A.; Zhang, T.; Hirano, A.; Imanishi, N.; Yamamoto, O.; Takeda, Y. Synthesis of Garnet-Type $Li_{7-x}La_3Zr_2O_{12-1/2x}$ and Its Stability in Aqueous Solutions. *Solid State Ionics* **2011**, *183* (1), 48−53.

(11) Bernstein, N.; Johannes, M. D.; Hoang, K. Origin of the Structural Phase Transition in $Li_7La_3Zr_2O_{12}$. *Phys. Rev. Lett.* **2012**, *109* (20), 205702.

(12) Inada, R.; Kusakabe, K.; Tanaka, T.; Kudo, S.; Sakurai, Y. Synthesis and Properties of Al-Free $Li_{7-x}La_3Zr_{2-x}Ta_xO_{12}$ Garnet Related Oxides. *Solid State Ionics* **2014**, *262*, 568−572.

(13) Miara, L. J.; Ong, S. P.; Mo, Y.; Richards, W. D.; Park, Y.; Lee, J.-M.; Lee, H. S.; Ceder, G. Effect of Rb and Ta Doping on the Ionic Conductivity and Stability of the Garnet Li_{7+2x-y} $(La_{3-x}Rb_x)$-$(Zr_{2-y}Ta_y)O_{12}$ ($0 \le x \le 0.375$, $0 \le y \le 1$) Superionic Conductor: A First Principles Invest. *Chem. Mater.* **2013**, *25* (15), 3048−3055.

(14) Allen, J. L.; Wolfenstine, J.; Rangasamy, E.; Sakamoto, J. Effect of Substitution (Ta, Al, Ga) on the Conductivity of $Li_7La_3Zr_2O_{12}$. *J. Power Sources* **2012**, *206*, 315−319.

(15) Galven, C.; Fourquet, J.; Crosnier-Lopez, M.-P.; Le Berre, F. Instability of the Lithium Garnet $Li_7La_3Sn_2O_{12}$: Li^+/H^+ Exchange and Structural Study. *Chem. Mater.* **2011**, *23* (7), 1892−1900.

(16) Ramakumar, S.; Satyanarayana, L.; Manorama, S. V.; Murugan, R. Structure and Li^+ Dynamics of Sb-Doped $Li_7La_3Zr_2O_{12}$ Fast Lithium Ion Conductors. *Phys. Chem. Chem. Phys.* **2013**, *15* (27), 11327−11338.

(17) Wolfenstine, J.; Ratchford, J.; Rangasamy, E.; Sakamoto, J.; Allen, J. L. Synthesis and High Li-Ion Conductivity of Ga-Stabilized Cubic $Li_7La_3Zr_2O_{12}$. *Mater. Chem. Phys.* **2012**, *134* (2−3), 571−575.

(18) Rangasamy, E.; Wolfenstine, J.; Allen, J.; Sakamoto, J. The Effect of 24c-Site (A) Cation Substitution on the Tetragonal−Cubic Phase Transition in $Li_{7-x}La_{3-x}A_xZr_2O_{12}$ Garnet-Based Ceramic Electrolyte. *J. Power Sources* **2013**, *230*, 261−266.

(19) Dhivya, L.; Janani, N.; Palanivel, B.; Murugan, R. Li^+ Transport Properties of W Substituted $Li_7La_3Zr_2O_{12}$ Cubic Lithium Garnets. *AIP Adv.* **2013**, *3* (8), 082115.

(20) Huang, M.; Dumon, A.; Nan, C.-W. Effect of Si, In and Ge Doping on High Ionic Conductivity of $Li_7La_3Zr_2O_{12}$. *Electrochem. Commun.* **2012**, *21*, 62−64.

(21) Thangadurai, V.; Kaack, H.; Weppner, W. J. F. Novel Fast Lithium Ion Conduction in Garnet-Type $Li_5La_3M_2O_{12}$ (M: Nb, Ta). *ChemInform* **2003**, *34* (27), 437−440.

(22) Thangadurai, V.; Weppner, W. $Li_6ALa_2Nb_2O_{12}$ (A = Ca, Sr, Ba): A New Class of Fast Lithium Ion Conductors with Garnet-Like Structure. *J. Am. Ceram. Soc.* **2005**, *88* (2), 411−418.

(23) Thangadurai, V.; Weppner, W. Investigations on Electrical Conductivity and Chemical Compatibility between Fast Lithium Ion Conducting Garnet-like $Li_6BaLa_2Ta_2O_{12}$ and Lithium Battery Cathodes. *J. Power Sources* **2005**, *142* (1−2), 339−344.

(24) Baral, A. K.; Narayanan, S.; Ramezanipour, F.; Thangadurai, V. Evaluation of Fundamental Transport Properties of Li-Excess Garnet-Type $Li_{5+2x}La_3Ta_{2-x}Y_xO_{12}$ (x = 0.25, 0.5 and 0.75) Electrolytes Using AC Impedance and Dielectric Spectroscopy. *Phys. Chem. Chem. Phys.* **2014**, *16*, 11356−11365.

(25) Gupta, A.; Murugan, R.; Paranthaman, M. P.; Bi, Z.; Bridges, C. A.; Nakanishi, M.; Sokolov, A. P.; Han, K. S.; Hagaman, E. W.; Xie, H.; Mullins, C. B.; Goodenough, J. B. Optimum Lithium-Ion Conductivity in Cubic $Li_{7-x}La_3Hf_{2-x}Ta_xO_{12}$. *J. Power Sources* **2012**, *209*, 184−188.

(26) Rangasamy, E.; Wolfenstine, J.; Sakamoto, J. The Role of Al and Li Concentration on the Formation of Cubic Garnet Solid Electrolyte of Nominal Composition $Li_7La_3Zr_2O_{12}$. *Solid State Ionics* **2012**, *206*, 28−32.

(27) Kotobuki, M.; Kanamura, K.; Sato, Y.; Yoshida, T. Fabrication of All-Solid-State Lithium Battery with Lithium Metal Anode Using Al_2O_3-Added $Li_7La_3Zr_2O_{12}$ Solid Electrolyte. *J. Power Sources* **2011**, *196* (18), 7750−7754.

(28) Li, Y.; Han, J.-T.; Wang, C.-A.; Vogel, S. C.; Xie, H.; Xu, M.; Goodenough, J. B. Ionic Distribution and Conductivity in Lithium Garnet $Li_7La_3Zr_2O_{12}$. *J. Power Sources* **2012**, *209*, 278−281.

(29) Buschmann, H.; Dolle, J.; Berendts, S.; Kuhn, A.; Bottke, P.; Wilkening, M.; Heitjans, P.; Senyshyn, A.; Ehrenberg, H.; Lotnyk, A.; Duppel, V.; Lorenz, K.; Janek, J. Structure and Dynamics of the Fast Lithium Ion Conductor "$Li_7La_3Zr_2O_{12}$". *Phys. Chem. Chem. Phys.* **2011**, *13*, 19378−19392.

(30) Düvel, A.; Kuhn, A.; Robben, L.; Wilkening, M.; Heitjans, P. Mechanosynthesis of Solid Electrolytes: Preparation, Characterization, and Li Ion Transport Properties of Garnet-Type Al-Doped $Li_7La_3Zr_2O_{12}$ Crystallizing with Cubic Symmetry. *J. Phys. Chem. C* **2012**, *116* (29), 15192−15202.

(31) Rettenwander, D.; Geiger, C. A.; Amthauer, G. Synthesis and Crystal Chemistry of the Fast Li-Ion Conductor $Li_7La_3Zr_2O_{12}$ Doped with Fe. *Inorg. Chem.* **2013**, *52* (14), 8005−8009.

(32) Hubaud, A. A.; Schroeder, D. J.; Key, B.; Ingram, B. J.; Dogan, F.; Vaughey, J. T. Low Temperature Stabilization of Cubic

DOI: 10.1021/acs.chemmater.5b01023
Chem. Mater. 2015, 27, 4040−4047

($Li_{7-x}Al_{x/3}$)$La_3Zr_2O_{12}$: Role of Aluminum during Formation. *J. Mater. Chem. A* **2013**, *1* (31), 8813.
(33) Takada, K.; Ohta, N.; Zhang, L.; Fukuda, K.; Sakaguchi, I.; Ma, R.; Osada, M.; Sasaki, T. Interfacial Modification for High-Power Solid-State Lithium Batteries. *Solid State Ionics* **2008**, *179* (27−32), 1333−1337.
(34) Kotobuki, M.; Munakata, H.; Kanamura, K.; Sato, Y.; Yoshida, T. Compatibility of $Li_7La_3Zr_2O_{12}$ Solid Electrolyte to All-Solid-State Battery Using Li Metal Anode. *J. Electrochem. Soc.* **2010**, *157* (10), A1076.
(35) Schwenzel, J.; Thangadurai, V.; Weppner, W. Developments of High-Voltage All-Solid-State Thin-Film Lithium Ion Batteries. *J. Power Sources* **2006**, *154* (1), 232−238.
(36) Ewald, P. P. Die Berechnung Optischer Und Elektrostatischer Gitterpotentiale. *Ann. Phys.* **1921**, *369*, 253−287.
(37) Ong, S. P.; Richards, W. D.; Jain, A.; Hautier, G.; Kocher, M.; Cholia, S.; Gunter, D.; Chevrier, V. L.; Persson, K. A.; Ceder, G. Python Materials Genomics (pymatgen): A Robust, Open-Source Python Library for Materials Analysis. *Comput. Mater. Sci.* **2013**, *68*, 314−319.
(38) *Inorganic Crystal Structure Database (ICSD), v. 2012*; The National Institutes of Science and Technology (NIST), Fachinformationszentrum Karlsruhe (FIZ). Available via the Internet at: http://www.fiz-karlsruhe.com/icsd_home.html.
(39) Hautier, G.; Fischer, C.; Ehrlacher, V.; Jain, A.; Ceder, G. Data Mined Ionic Substitutions for the Discovery of New Compounds. *Inorg. Chem.* **2011**, *50*, 656−663.
(40) Adams, S.; Rao, R. P. Ion Transport and Phase Transition in $Li_{7-x}La_3(Zr_{2-x}M_x)O_{12}$ (M = Ta^{5+}, Nb^{5+}, x = 0, 0.25). *J. Mater. Chem.* **2012**, *22*, 1426−1434.
(41) Perdew, J.; Emzerhof, M.; Burke, K. Rationale for Mixing Exact Exchange with Density-Functional Approximations. *J. Chem. Phys.* **1996**, *105* (22), 9982−9985.
(42) Kresse, G.; Furthmüller, J. Efficient Iterative Schemes for Ab Initio Total-Energy Calculations Using a Plane-Wave Basis Set. *Phys. Rev. B. Condens. Matter* **1996**, *54* (16), 11169−11186.
(43) Blöchl, P. Projector Augmented-Wave Method. *Phys. Rev. B* **1994**, *50*, 24.
(44) Geiger, C. A.; Alekseev, E.; Lazic, B.; Fisch, M.; Armbruster, T.; Langner, R.; Fechtelkord, M.; Kim, N.; Pettke, T.; Weppner, W. Crystal Chemistry and Stability of "$Li_7La_3Zr_2O_{12}$" Garnet: A Fast Lithium-Ion Conductor. *Inorg. Chem.* **2011**, *50* (3), 1089−1097.
(45) Rettenwander, D.; Blaha, P.; Laskowski, R.; Schwarz, K.; Bottke, P.; Wilkening, M.; Geiger, C. a.; Amthauer, G. DFT Study of the Role of Al^{3+} in the Fast Ion-Conductor $Li_{7-3x}Al_{3+x}La_3Zr_2O_{12}$ Garnet. *Chem. Mater.* **2014**, *26*, 2617−2623.
(46) Rettenwander, D.; Geiger, C. A.; Tribus, M.; Tropper, P.; Wagner, R.; Tippelt, G.; Lottermoser, W.; Amthauer, G. The Solubility and Site Preference of Fe in $Li_{7-3x}Fe_xLa_3Zr_2O_{12}$ Garnets. *J. Solid State Chem.* **2015**, DOI: 10.1016/j.jssc.2015.01.016.
(47) O'Callaghan, M. P.; Powell, A. S.; Titman, J. J.; Chen, G. Z.; Cussen, E. J. Switching on Fast Lithium Ion Conductivity in Garnets: The Structure and Transport Properties of $Li_{3+x}Nd_3Te_{2-x}Sb_xO_{12}$. *Chem. Mater.* **2008**, *20* (6), 2360−2369.
(48) Wang, Y.; Lai, W. High Ionic Conductivity Lithium Garnet Oxides of $Li_{7-x}La_3Zr_{2-x}Ta_xO_{12}$ Compositions. *Electrochem. Solid-State Lett.* **2012**, *15* (5), A68.
(49) Bruce, P. Ionic Conductivity of LISICON Solid Solutions, $Li_{2+2x}Zn_{1-x}GeO_4$. *J. Solid State Chem.* **1982**, *44* (3), 354−365.
(50) Alpen, U.; Bell, M.; Wichelhaus, W.; Cheung, K.; Dudley, G. Ionic-Conductivity of $Li_{14}Zn(GeO_4)_4$ (LISICON). *Electrochim. Acta* **1978**, *23* (12), 1395−1397.
(51) Bruce, P. G.; West, A. R. The A-C Conductivity of Polycrystalline LISICON, $Li_{2+2x}Zn_{1-x}GeO_4$, and a Model for Intergranular Constriction Resistances. *J. Electrochem. Soc.* **1983**, *130*, 662−669.
(52) Ping Ong, S.; Wang, L.; Kang, B.; Ceder, G. Li−Fe−P−O_2 Phase Diagram from First Principles Calculations. *Chem. Mater.* **2008**, *20* (5), 1798−1807.
(53) Mo, Y.; Ong, S. P.; Ceder, G. First Principles Study of the $Li_{10}GeP_2S_{12}$ Lithium Super Ionic Conductor Material. *Chem. Mater.* **2012**, *24*, 15−17.
(54) Ramaswamy, S.; Janani, N.; Murugan, R. Influence of Lithium Concentration on the Structure and Li^+ Transport Properties of Cubic Phase Lithium Garnets. *Dalton Trans.* **2015**, *44*, 539−552.
(55) Hitz, G. T.; Wachsman, E. D.; Thangadurai, V. Highly Li-Stuffed Garnet-Type $Li_{7+x}La_3Zr_{2-x}Y_xO_{12}$. *J. Electrochem. Soc.* **2013**, *160* (8), A1248−A1255.
(56) Lee, J.-M.; Kim, T.-Y.; Park, Y.-S.; Baek, S.-W.; Lee, J.-H. *Solid Ion Conductor, Solid Electrolyte Including the Same, Lithium Battery Including the Solid Electrolyte, and Method of Manufactureing the Solid Ion Conductor*. U.S. Patent No. US 20140227614 A1, Aug. 14, 2014.
(57) Kim, K. H.; Iriyama, Y.; Yamamoto, K.; Kumazaki, S.; Asaka, T.; Tanabe, K.; Fisher, C. A. J.; Hirayama, T.; Murugan, R.; Ogumi, Z. Characterization of the Interface between $LiCoO_2$ and $Li_7La_3Zr_2O_{12}$ in an All-Solid-State Rechargeable Lithium Battery. *J. Power Sources* **2011**, *196* (2), 764−767.
(58) Kotobuki, M.; Kanamura, K. Fabrication of All-Solid-State Battery Using $Li_5La_3Ta_2O_{12}$ Ceramic Electrolyte. *Ceram. Int.* **2013**, *39* (6), 6481−6487.
(59) Ohta, S.; Kobayashi, T.; Seki, J.; Asaoka, T. Electrochemical Performance of an All-Solid-State Lithium Ion Battery with Garnet-Type Oxide Electrolyte. *J. Power Sources* **2012**, *202*, 332−335.
(60) Lehmann, U.; Muller-Buschbaum, H. Ein Beitrag Zur Chemie Der Oxocobaltate(II): La_2CoO_4, Sm_2CoO_4. *Z. Anorg. Allg. Chem.* **1980**, *470* (1), 59−63.

DOI: 10.1021/acs.chemmater.5b01023
Chem. Mater. 2015, 27, 4040−4047